Nanoscale Advances

ROYAL SOCIETY OF CHEMISTRY

PAPER

View Article Online
View Journal | View Issue

Cite this: *Nanoscale Adv.*, 2023, **5**, 5094

A hybrid polymer protective layer with uniform Li^+ flux and self-adaption enabling dendrite-free Li metal anodes†

Chaohui We,[a] Jinxiang Deng,[b] Jianxiong Xing,[ab] Zihao Wang,[ab] Zhicui Song,[ab] Donghuan Wang,[a] Jicheng Jiang,[a] Xin Wang,[a] Aijun Zhou,[ab] Wei Zou[c] and Jingze Li *[ab]

Lithium (Li) metal is considered as an ideal negative electrode material for next-generation secondary batteries; however, the hideous dendrite growth and parasitic reactions hinder the practical applications of Li metal batteries. Herein, a hybrid polymer film composed of polyvinyl alcohol (PVA) and polyacrylic acid (PAA) is adopted as an artificial protective layer to inhibit the dendritic formation and side reactions in Li metal anodes. PVA with large quantities of polar functional groups can induce even distribution of Li ions (Li^+). Alternatively, PAA can *in situ* react with Li metal to form highly elastic and ionic conducting lithium polyacrylic acid (LiPAA), thereby enabling tight contact and flexible self-adaption with Li metal anodes. Therefore, such a rationally designed functional composite layer, with good binding ability and relatively high Li^+ conductivity, as well as excellent capability of homogenizing Li^+ flow, accordingly enables Li metal anodes to reveal dendrite-free plating/stripping behaviours and minimum volume variation. As a result, the PVA–PAA modified Li metal anode delivered stable cycling for 700 and 250 h, respectively, at current densities of 1 and 3 mA cm^{-2} under an areal capacity of 1 mA h cm^{-2}, in a carbonate ester-based electrolyte without any additive, exhibiting boosted cycling and rate performances. The Li anode with a functional PVA–PAA hybrid interlayer can maintain the dense and smooth texture without dendrite formation after long cycles. The full cell of Li|$LiFeO_4$ with our modified Li anode and a cathode with a high areal capacity of 2.45 mA h cm^{-2} delivers, change to achieved a long-term lifespan of 180 cycles at 1.0 C, with a capacity retention of 96.7%. This work demonstrates a simple and effective strategy of designing multi-functional artificial protective layers, targeting dendrite-free Li anodes.

Received 18th April 2023
Accepted 8th July 2023

DOI: 10.1039/d3na00248a

rsc.li/nanoscale-advances

Introduction

Owing to the ultra-high specific capacity (3860 mA h cm^{-2}) and low reduction potential (−3.04 V *vs.* the standard hydrogen electrode (SHE)), lithium (Li) metal has been recognized as a promising candidate for anodes of rechargeable Li metal batteries (LMBs).[1–4] Nevertheless, the detrimental dendrite growth and serious side reactions during cycling are two main obstacles in the way of commercial implementation of LMBs.[3,5] It is widely known that the solid interphase electrolyte (SEI) layer formed on the bare Li metal anode is fragile, which repeatedly breaks and grows over electrochemical cycling, resulting in nonuniform Li deposition with dendritic morphology.[6,7] Meanwhile, those parasitic reactions between the Li anode and electrolyte could rapidly consume the electrolyte and Li metal in each cycle, causing low coulombic efficiency (CE) and short lifespan of LMBs. Of note, the continuous formation of dendritic Li can even pierce through the separator, consequent to battery short-circuit and alarming safety hazards.[8–10]

Various endeavours have been devoted to addressing the above-mentioned issues related to Li metal anodes, which generally fall into two categories. One is the direct modification of the bulk structure of Li anodes *via* incorporating a three-dimensional framework,[11,12] synthesizing a dual phase Li alloy,[13,14] and constructing Li metal composites.[11,15] The interior scaffold can not only enhance the mechanical stability and retard the volume variation of the electrode, but can also act as the electrochemically active site to enlarge the surface area and regulate the Li deposition.[11] The other way is to optimize the surface conditions of the Li metal anode to achieve a robust

[a]*Yangtze Delta Region Institute (Huzhou), University of Electronic Science and Technology of China, Huzhou 313001, China. E-mail: lijingze@uestc.edu.cn*
[b]*School of Materials and Energy, University of Electronic Science and Technology of China, Chengdu 611731, China*
[c]*Lithium Resources and Lithium Materials Key Laboratory of Sichuan Province, Tianqi Lithium Co., Ltd., Chengdu 610093, China*

† Electronic supplementary information (ESI) available. See DOI: https://doi.org/10.1039/d3na00248a

interface with low interfacial impedance *via* tunning electrolyte components,[16,17] introducing electrolyte additives,[7,18] and covering the anode with an artificial protective layer.[19,20]

Recently, constructing an artificial SEI layer has attracted extensive attention, due to the advantageous simplicity in the preparation process and efficacy in suppressing dendrite growth. Typically, the protective films are composed of inorganic insulators,[21,22] inorganic ion conductors,[23–26] Li alloys,[27–30] polymers,[31–33] or composites.[19,47] Inorganic protective films like Al_2O_3 (ref. 21) and Li_3PO_4 (ref. 24) with a high Young's modulus can effectively prevent the penetration of Li dendrites; however, the thin inorganic films tend to become pulverized, due to the poor flexibility and the rapidly accumulated internal stress, induced by the large volume evolution after multiple Li stripping/depositing cycles. Alternatively, the polymer film seems a good choice considering its high elasticity, film-forming properties and easy synthesis. Polymers like polyvinyl alcohol (PVA),[33] hydroxypropyl methyl cellulose (HPMC),[34] and β-phase polyvinylidene difluoride (β-PVDF)[35] with large quantities of polar functional groups, enable strong interaction with Li ions (Li^+), guiding uniform Li deposition. Wu and co-workers demonstrated a highly tight PVA layer on the Cu/Li surface to realize a dense deposition of Li without grain boundaries and voids, induced by the confinement effect and lithiophilic feature of PVA coating.[32] Similarly, Cao's group introduced a viscoelastic HPMC interlayer with excellent lithiophilicity and electrochemical and mechanical stability, enabling dendrite-free and zero volume expansion Li anodes.[34] Nevertheless, the relatively low ionic conductivity of most polymer films limits the electrochemical performance of Li metal anodes, especially at high current density.[36,37] In line with this, the inorganic species are often incorporated into the polymer films as fillers. For instance, adding LiF particles to poly(ethylene oxide) (PEO),[38] introducing Li bis-trifluoromethyl sulfonate (LiTFSI) salt into polyethylene vinyl alcohol-β-acrylonitrile ether (EBC),[20] and joining Cu_3N nanoparticles to styrene butadiene rubber (SBR)[39] have been reported as effective synergised interlayers for Li anodes. Despite this, the detachment of the artificial protective layer during long cycles, resulting from the low binding ability between the coating film and Li metal, is still a major challenge yet to be solved. Generally, polymer films like polyacrylic acid (PAA),[40] pentanoic acid,[6] pendant PEO segments and ureido-pyrimidinone (UPy)[41] with strong binding ability, can *in situ* react with Li metal. One can expect that the combination of desired properties including high binding ability, strong Li^+ homogenizing capability and superior ionic conductivity in the designed integrated protection layer could effectively resolve the issues of Li dendrite growth, volume change and side reactions.

Herein, we rationally design an artificial hybrid protective layer composed of polyvinyl alcohol (PVA) and PAA *via* a one-step *in situ* reaction. PVA with sufficient hydroxyl groups can firmly bond with Li atoms to avoid the ion agglomeration around Li protrusions and achieve even Li deposition. Meanwhile, PVA is a widely used synthetic polymer with low-cost, and excellent thermal, mechanical, and chemical stabilities, coupled with good film-forming properties.[32,39,41] Unfortunately, the relatively low ionic conductivity and inferior binding ability with Li metal of PVA can retard the Li^+ transportation under high current density and induce shortened lifespan of LMBs. Alternatively, PAA can *in situ* react with Li metal to form highly stretchable and favourable ionic conducting lithium polyacrylic acid (LiPAA) showing enhanced contact with Li metal and excellent stability, consequently adapting to volumetric change over multiple Li dissolution/deposition processes.[43–45] Accordingly, by mixing PVA and PAA as an artificial protective layer, the advantages of uniform Li^+ flux from PVA coupled with favourable Li^+ conductivity and robust binding ability of LiPAA are synergized. Therefore, when such a hybrid polymer film is applied in symmetric Li|Li cells at various current densities, the cell exhibits enhanced cycling stability (700 h at 3 mA cm^{-2}/1 mA h cm^{-2}) in a carbonate ester-based electrolyte without any additive. While the PVA–PAA film is coated on the Cu current collector, Li|Cu cells can smoothly cycle for 200 cycles under 3 mA cm^{-2}/1 mA h cm^{-2} with a high coulombic efficiency (CE) of 97.5%. Our modified Li anode can readily resist the volume fluctuation and prevent dendrite growth over long cycling. In addition, when paired with a high areal loading $LiFePO_4$ cathode (about 2.45 mA h cm^{-2}), the Li|$LiFeO_4$ cell with a PVA–PAA coated Li anode displays a long lifespan of 180 cycles at 1.0 C, with a low-capacity decay percentage of 3.3%.

Experimental

Preparation of PVA–PAA coated Cu foil

PVA and PAA were mixed in different weight ratios (PVA : PAA = 1 : 0; 8 : 1; 4 : 1; 2 : 1; 1 : 1; 1 : 4; 0 : 1) and dissolved in dimethyl sulfoxide (DMSO) under a concentration of 1 wt%. A uniform mixed solution was obtained after vigorously stirring for 24 h. A glass rod was utilized to cast the solution on Cu foil. The coated Cu foil was then dried in an oven at 60 °C for 72 h to ensure the complete volatilization of DMSO solvent, and cut into a round disc of 19 mm diameter after drying.

Preparation of PVA–PAA coated Li metal

The coating process on Li foil was carried out in a glove box. Firstly, the native passivation film on the Li metal surface was removed mechanically *via* scratching, and then the Li sheet was pressed into a disc with a diameter of 12 mm, and 20 μL of the mixed solution is added dropwise on the Li surface with a pipette, and dried naturally in a glove box. The thickness of the coating layer was controlled by adding dropwise different volumes on the Li foil.

Electrochemical measurements and characterization

Carbonate-based electrolyte was composed of 1 M lithium hexafluorophosphate ($LiPF_6$) dissolved in a 1 : 1 (v/v) mixture of ethylene carbonate (EC) and dimethyl carbonate (DEC) without any additive. Ether-based electrolyte consists of 1 M LiTFSI in a 1 : 1 (v/v) mixture of 1, 3-dioxolane and 1, 2 dimethoxyethane with 2 wt% $LiNO_3$ additives. In this work, Li|Cu cells were tested in the ether-based electrolyte, while symmetric cells and Li|LFP cells were measured in the carbonate-based electrolyte. The areal capacity of our LiFePO4 cathode was about

2.45 mA h cm^{-2}, which is equal to the areal loading of 17.1 mg cm^{-2}. The corresponding E/S ratio applied in our articles is 5 μL mg^{-1}. Galvanostatic charging/discharging was conducted on a LAND CT2001A instrument at different current densities. The asymmetric Li|Cu batteries were tested in the ether-based electrolyte, under a certain charge time, and a discharge cut-off voltage of 1.0 V for the Li stripping/deposition process. The Li|LFP cells were cycled in a voltage window between 2.20 and 3.85 V. The rate performances of LFP batteries were tested at 0.1, 0.2, 0.5, 1.0 and 2.0 C each for 5 cycles, and then tested at 1.0 C for several cycles. All cells were assembled in an argon-filled glove box with less than 0.1 ppm oxygen and 0.1 ppm H_2O. Electrochemical Impedance spectroscopy (EIS) measurement was carried out on an electrochemical workstation (Shanghai Chenhua CHI660C) in a frequency range from 100 kHz to 100 MHz with an amplitude of 10 mV. The top-view and side-view Scanning Electron Microscopy (SEM) and elemental mapping images were collected from a JEOLJSM-6490LV at 20 kV. X-ray diffraction (XRD) patterns were recorded with Cu Kα (λ = 0.154056 nm) radiation at 101 min^{-1} over a 2θ range from 10 to 90°.

Ionic conductivity measurements

A typical coin cell with stainless steel as the block electrode was assembled and tested in a frequency range from 100 kHz to 100 MHz with an amplitude of 10 mV. 20 μL of ester solution was applied as the electrolyte. The ionic conductivity can be obtained from the below equation:

$$\sigma = L/R_b S$$

where σ (S cm^{-1}) stands for the ionic conductivity, L (cm) represents the thickness of the polymer electrolyte, R_b (Ω) means the intrinsic impedance of the polymer electrolyte, and S (cm^2) indicates the contact area between the stainless steel and polymer electrolyte.

Results and discussion

The fabrication process of the surface coating is displayed in Fig. 1a. The PVA–PAA layer on Li foil can be spontaneously produced by drop casting the PVA–PAA solution dissolved in DMSO with a mass fraction of 1 wt%, followed by natural evaporation in a glove box (Fig. 1a). With such a hybrid film coated on the Li foil surface, Li^+ flux can be effectively homogenized, leading to smooth deposition behaviours, whilst the dendrite gradually grows on bare Li foil (Fig. 1b). Fig. 2a and b show the optical and SEM images of Cu foils with and without PVA–PAA coating. The colour of the Cu foil turns brown and the surface becomes smoother after casting PVA–PAA, as compared to bare Cu. The cross-sectional SEM image in Fig. 2c reveals that the thickness of the PVA–PAA protection layer on Cu foil is around 1.20 μm. Upon casting the PVA–PAA foil, the modified Li foil exhibits a glossier texture with a brighter colour and even surface (Fig. 2d and e). The thickness of the PVA–PAA protection layer on Li foil is also around 1.20 μm, as shown in Fig. 2f,

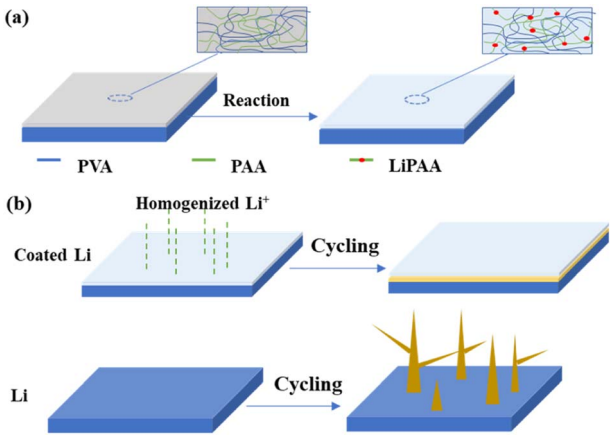

Fig. 1 (a) Fabrication process of Li metal coated with the PVA–PAA film. (b) Morphology comparison of Li metal with and without the PVA–PAA layer.

indicating that the reaction between metallic Li and PAA has no impact on the film thickness.

The proportion of PVA and PAA as well as thickness of the coating layer are vital indices for the electrochemical performance of the PVA–PAA hybrid film in ester electrolyte. Therefore, a series of PVA–PAA mixtures in various weight ratios (PVA : PAA = 1 : 0; 8 : 1; 4 : 1; 2 : 1; 1 : 4; 0 : 1) were dissolved in DMSO under a weight percentage of 1 wt%. From Fig. S1a,† Cu foil with only PVA coating can operate for 220 cycles with a CE of 98.0%. When a small amount of PAA is added to PVA (PAA : PVA = 1 : 8), the cycling behaviour was significantly improved, due to the addition of PVA giving rising to LiPAA with relatively high ionic conductivity.[42–44] The optimal electrochemical performance can be observed (CE: 98.5% after 300 cycles at 1 mA cm^{-2}, 1 mA h cm^{-2}), when the weight ratio of PVA to PAA increases to 4 : 1. However, as the weight of PAA further increased, the length of the cycling period was lowered. Such a phenomenon indicates that the over-dose of PAA in PVA would deteriorate the film integrity of the hybrid film, thereby failing to isolate the electrolyte and

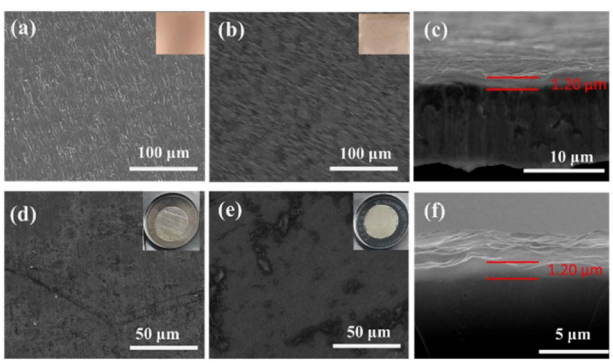

Fig. 2 Optical and SEM images of (a) bare Cu foil and (b) PVA–PAA coated Cu foil. (c) Cross-sectional SEM image of PVA–PAA coated Cu foil. Optical and SEM images of (d) bare Li and (e) PVA–PAA coated Li. (f) Cross-sectional SEM image of PVA–PAA coated Li.

inhibit Li dendrite growth. Hence, the weight ratio of 4 : 1 was selected as the optimal parameter, as both decent ionic conductivity and distributed Li^+ flux can be synergized in the ultimate robust hybrid PVA–PAA film. When increasing the current to 3 mA cm^{-2}, the PVA–PAA layer with a weight ratio of 4 : 1 also exceled its counterparts (Fig. S1b†). Subsequently, Cu foil cast with PVA–PAA of different thickness was measured to investigate the appropriate coating thickness (PVA–PAA-1, PVA–PAA-2, PVA–PAA-3, and PVA–PAA-4). Clearly, the cycling lifespan of PVA–PAA-2@Cu foil was longer, as compared to its counterparts (Fig. S2†). The over-thin layer tends to contain defects inside the structure, failing to isolate the electrolyte and resist the volume change over cycling. The over-thick coating layer may lead to insufficient structural integrity, and the consequent over-long transport path of ions could reduce the evenness of Li deposition.

Upon the optimization of preparation parameters, the CE of bare Cu foil, PVA, PAA and PAA–PVA (1 : 4) coated Cu foil was evaluated at a current density of 1 mA cm^{-2} and areal capacity of 1 mA h cm^{-2}. Prior to the test, the ionic conductivity of different coating layers was evaluated with the precursor solution drop casting on stainless steel. 20 μL of ester solution was applied as the supporting electrolyte. As exhibited in Fig. S3,† the ionic conductivity of the ester electrolyte was higher (3.18×10^{-4} S cm^{-1}), as compared to PAA (1.06×10^{-4} S cm^{-1}), PVA (1.59×10^{-6} S cm^{-1}) and PAA–PVA films (5.03×10^{-5} S cm^{-1}). The resistance in the high frequency range in Fig. S4† also followed the trend in Fig. S3† (PVA > PVA–PAA > PAA > liquid electrolyte). The thickness of the coating layer over the test is about 1.20 μm. Distinctly, the incorporation of PAA can improve the ionic conductivity of the PVA layer, favourable for the fast transport of Li^+ and subsequent homogeneous growth. Additionally, the stress–strain profiles of PVA and PVA–PAA films are shown in Fig. S5.† As compared to the PVA film, the coating layer of the PVA–PAA film was markedly more stretchable (289% strain to its initial length), effectively adapting to the volume fluctuation without brittle fracture.[42,44]

From Fig. 3a and b, the Li|Cu cell can only cycle for 120 and 40 cycles, respectively, at 1 mA cm^{-2}/1 mA h cm^{-2} and 3 mA cm^{-2}/1 mA h cm^{-2}, as the non-uniform deposition of Li on pure Cu can induce the formation of dendrites and dead Li, thereby resulting in short cycle life and low CE. After coating the PVA film with the function of uniform Li^+ flux on the Cu foil, it can cycle stably for 220 and 90 cycles at 1 mA cm^{-2}/1 mA h cm^{-2} and 3 mA cm^{-2}/1 mA h cm^{-2}, respectively. In stark contrast, the PVA–PAA casted Cu foil can smoothly operate for 300 (98.5%) and 200 (97.5%) cycles, respectively, under 1 mA cm^{-2}/1 mA h cm^{-2} and 3 mA cm^{-2}/1 mA h cm^{-2}, demonstrating enhanced cycling stability as compared to the counterpart. Additionally, the CE of the as-prepared hybrid PVA–PAA was tested in ester electrolyte, as exhibited in Fig. S6,† where the CE of protected Cu foil clearly outperformed that of bare Cu foil. Such improvement can be attributed to the superior Li^+ transmission and distribution capability of the hybrid PAA–PVA film, enabling fast and

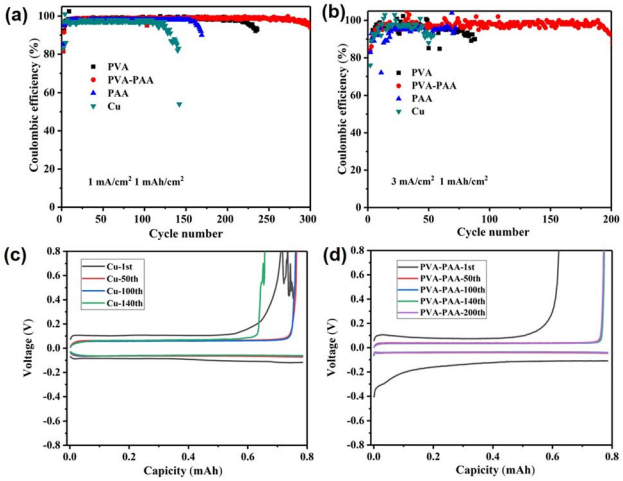

Fig. 3 CE comparison of Li/Cu cells based on PVA, PVA–PAA, PAA coated Cu and bare Cu at current densities of (a) 1 mA cm^{-2} and (b) 3 mA cm^{-2} with a fixed capacity of 1 mA h cm^{-2}. Voltage profiles of cells using (c) Cu foil and (d) PVA–PAA coated Cu foil at different cycling states at 1 mA cm^{-2} and 1 mA h cm^{-2}.

reversible Li redox reactions. The following voltage–capacity profiles are disclosed in Fig. 3c and d. Although the initial capacity of both Cu and PAA–PVA@Cu was relatively low, PAA–PVA@Cu demonstrated the increased charge capacity and CE in the subsequent cycles. The inferior capacities of Cu foil and PAA–PVA@Cu in the 1st cycle were due to the generation of a SEI and LiPAA, respectively. In the remaining cycling, the occurrence of parasitic reactions and dead Li on bare Cu consumed a large amount of active Li, whilst PAA–PVA casted Cu foil can inhibit the side reactions and enable homogeneous Li nucleation. Furthermore, the relatively high charge capacity and low polarisation voltage of the cell with PAA–PVA coated Cu foil after 200 cycles, in compared to Cu, suggest a stabilised interface induced by the hybrid polymer coating.

In order to explore the influence of PVA–PAA coating on the behaviour of Li deposition, a capacity of 5 mA h cm^{-2} Li was

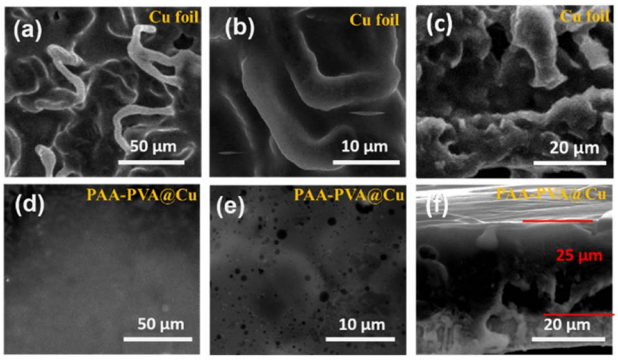

Fig. 4 (a and b) Surface and (c) cross-sectional morphology of Li deposition on Cu; (d and e) surface and (f) cross-sectional morphology of Li deposition on PVA–PAA coated Cu, after depositing 5 mA h cm^{-2} of Li with a current density of 0.5 mA cm^{-2}.

deposited on bare and coated Cu at a current density of 0.5 mA cm^{-2}. As shown in Fig. 4a and b, the Li deposition on Cu foil was very uneven and ends up in dendritic formation. From the cross-sectional view in Fig. 4c and S7,† the thickness of Li deposition on bare Cu was about 64 μm, much larger than the theoretical thickness (25 μm), suggestive of a loose structure of deposited Li. In contrast, the deposited Li on the PVA–PAA coated Cu foil shows a flat coating surface with dense Li growth below (the thickness is 25 μm, Fig. 4d–f). This indicates that Li^+ can transport though the PVA–PAA polymer layer and distribute homogeneously to achieve uniform nucleation and dissolution behaviours, thereby suppressing dendrite growth and buffering dimensional variation. Furthermore, the deposited Li was electrochemically extracted from the coated Cu electrode under the same conditions. From the SEM image in Fig. S8,† the coating layer on Cu foil returned to the original state, and becomes smoother and flatter after the Li extraction, due to the reaction between PAA and Li. This indicates that such a mechanically robust film can induce uniform deposition of Li and resist the volume change in the subsequent cycling process.

The application of the hybrid PAA–PVA polymer layer directly on Li metal was also investigated *via* a symmetric cell configuration. Similarly, the coating layer thickness on Li foil was assessed upon adjusting the drop volume of precursor solution to explore the optimal parameter. Under a current density of 3 mA cm^{-2} with a fixed capacity of 1 mA h cm^{-2} in carbonate-based electrolyte, the symmetric cell of PVA–PAA-30 on Li foil maintained a longer cycling period and smaller polarization hysteresis, in comparison to the reference cells (Fig. S9†). Hence, a dose of 30 μL was chosen as the optimal condition for modifying the surface of Li foil, with a thickness of 1.2 μm, equalling the optimal thickness of the coating on Cu foil. An equivalent circuit (Fig. S10a† inset) was used to fit these impedance spectra using ZView software. The R_S, R_f, and R_{CT} respectively stand for the bulk resistance of the cell, surface passivation layer, and charge-transfer process.[46,47] The fitting results of overall resistance are displayed in Table S1.† The initial impedance of the Li|Li symmetric cell was 415.2 Ω. After 50 cycles, the impedance reduces to 175.1 Ω, due to the activation process, and then gradually increases in the subsequent cycles (100^{th} cycle: 190.0 Ω; 200^{th} cycle: 253.7 Ω). The underneath reasons lie in the brittle original SEI continuing to crack and grow during the cycle, resulting in non-uniform current distribution and high Li^+ flux near cracks. The growth of dendrite Li and accumulation of dead Li exhibit high impedance, as shown in the Nyquist plot. Despite markedly large initial impedance of the PVA–PAA coated Li|Li symmetric cell (762.4 Ω) in the 1^{st} cycle, as compared to the Li|Li cell, due to relatively low conductivity of the coating layer in contrast to liquid electrolyte, the modified cell maintained a stable small impedance in the following circulation (95.1, 88.1 and 93.2 Ω in the 50^{th}, 100^{th} and 200^{th} cycles, respectively). The steadied trend of resistance of the modified Li cell can directly suggest the successfully in-built robust film on the anode surface, which can distribute Li^+ flux rapidly and homogeneously to resist the dimensional expansion and dendritic growth. As shown in Fig. 5a and b and S11,† the

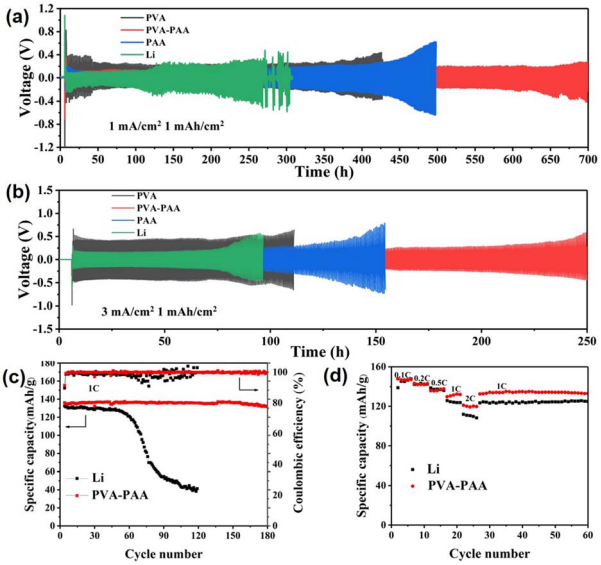

Fig. 5 Cycle performances of symmetric cells based on PVA, PVA–PAA, PAA coated Li and bare Li at current densities of (a) 1 mA cm^{-2} and (b) 3 mA cm^{-2} with a fixed capacity of 1 mA h cm^{-2}. (c) Cycle at 1.0 C and (d) rate performance of bare Li||LFP and PVA–PAA coated Li||LFP cells.

voltage hysteresis of the pure Li|Li symmetric cell increased significantly when cycling to 120 h, and a short circuit occurred at 260 h. In contrast, the coated Li||Li cell shows boosted long-cycle performance of stable operation for 700 and 250 h under 1 mA cm^{-2}/1 mA h cm^{-2} and 3 mA cm^{-2}/1 mA h cm^{-2}, respectively. Additionally, the largest polarization hysteresis of the symmetric cell with PVA coating validates the inadequate ionic conductivity of PVA, unable to rapidly transport Li^+, particularly under high current density. The cycling behaviours were consistent with electrochemical impedance spectroscopy (EIS) data in Fig. S10 and Table S1.† There are three possible causes for such observation: (i) the fine coating layer can provide a stable interface in between the Li surface and electrolyte, to regulate the Li^+ flux and prevent side reactions; (ii) the favourable ionic conductivity of the hybrid film can ensure the rapid transmission of Li^+, instead of local accumulation; (iii) the PVA–PAA layer with a high binding ability between the coating layer and Li metal, coupled with considerable mechanical strength and flexibility, can guarantee the tight contact of the polymer film and anode, and well adapt to volume changes during long cycles. Those synergistic effects can enable rational Li nucleation/dissolution behaviour and consequently long lifespan.

The outstanding performances of PVA–PAA coated Li in symmetric cells demonstrate its high feasibility in practical cells. Herein, a commercial $LiFeO_4$ cathode with an areal capacity of 2.45 mA h cm^{-2} was adopted to pair with the PVA–PAA coated Li anode. As shown in Fig. 5c, the PVA–PAA coated Li|LFP cell delivered a high reversible capacity of 148.2 mA h g^{-1} at 1.0 C (1.92 mA cm^{-2}) and maintained a discharge capacity of 124.8 mA h g^{-1} after 180 cycles, with a retention rate of 96.7%. In contrast, the capacity of the

Li|LFP cell decays from 148.8 to 74.4 mA h g^{-1} after 65 cycles at 1.0 C. The Galvanostatic charge/discharge curves in Fig. S12† showed the polarization voltage of the Li|LFP cell markedly increased after multiple cycles, probably due to the accumulation of dead Li impeding the transfer of Li at the interfaces, and resulting in low CE and fast capacity decay. The rate performances of the full cells were measured at different current densities (Fig. 5d). The modified Li|LFP cell delivered a higher specific capacity of 147.8, 143.1, 135.8, 130.4, and 121.2 mA h g^{-1} respectively at 0.1, 0.2, 0.5, 1.0 and 2.0 C, in comparison to the Li|LFP cell (145.2, 142.5, 138.5, 125.2, and 111.3 mA h g^{-1} at 0.1, 0.2, 0.5, 1.0 and 2.0 C, respectively). The increased capacity difference of the two cells along with the rise of applied current suggests the generation of dendrites and dead Li on unmodified Li can aggravate the uneven deposition of Li, particularly at a high rate.

To further illustrate the role of the PVA–PAA protective layer, post-mortem SEM images were collected to study the morphology of the Li metal anode after 50 cycles at a current density of 1 mA cm^{-2} with a fixed capacity of 1 mA h cm^{-2}. From Fig. 6a–c, vast quantities of dendrites and dead Li were formed on the uncoated Li metal anode, caused by uneven Li deposition and serious side-reactions between Li metal and electrolyte. In contrast, the surface of modified Li anode revealed a flat and dense texture, with the PVA–PAA film tightly coating on the top, effectively isolating the electrolyte and offering a stabilized interface (Fig. 6d–f).

The structural evolutions of bare Li and PVA–PAA coated Li are displayed in Fig. 7 to demonstrate the protection mechanism of the functional polymer layer. Owing to the nature of high reactivity and ultralow reduction potential, Li metal tends to interact with the electrolyte to form an SEI layer in the initial cycle. During Li plating, the uneven distribution of Li^+ flux and the rough electrode surface can cause nonuniform Li deposition and dendrite growth. The accompanying large dimensional fluctuation would rupture the fragile SEI and expose fresh Li, which can further react with the electrolyte to form a new SEI. Such a process of continuous cracking and repair of the SEI would repeat in the subsequent cycles, over-consuming active Li and electrolyte, corroding the anode surface, and producing enormous dead Li. In the end, the Li anode will become porous or even pulverized. In stark contrast, when PVA–PAA was applied as an artificial SEI on the top of Li surface, the above-mentioned challenges could be addressed. The superior Li^+ distribution capability, the decent mechanical strength and good film-forming properties of PVA as well as good ionic conductivity and tight contact with Li metal of PAA were rationally incorporated in the hybrid film. Hence, the PVA–PAA layer can enable strong binding with the Li anode, homogeneous Li^+ flux and a rapid Li^+ transportation rate, achieving uniform and compact deposition of Li without dendrite formation and volume fluctuation.

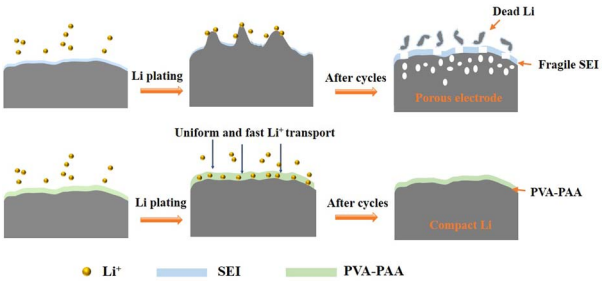

Fig. 7 Schematic illustration of the cycling process of the Li metal anode with and without the PVA–PAA coating layer.

Conclusions

In summary, we have successfully demonstrated that the as-prepared PVA–PAA hybrid coating layer can effectively stabilize the electrode/electrolyte interface and inhibit the growth of Li dendrites. Therefore, a large deposition of Li (5 mA h cm^{-2}) on coated Cu foil can obtain a uniform and dense electrode. The Li|Cu half cells can stably cycle for 300 cycles at 1 mA cm^{-2}/1 mA h cm^{-2}, with a high CE of 98.5%. The symmetric cell with PVA–PAA coating can continuously operate for 250 h at a high current of 3 mA cm^{-2} under an areal capacity of 1 mA h cm^{-2}. In addition, when applied to commercial LFP cathodes, the PVA–PAA@Li|LFP cell displayed excellent rate and cycling performances (180 cycles at 1.0 C with a capacity retention of 96.66%; 121.2 mA h g^{-1} at 2.0 C). The reasons behind the phenomena are as follows: (1) the PVA–PAA coating layer can isolate the electrolyte and reactive Li metal to prevent side-reactions and over-consumption of active materials; (2) the PVA–PAA coating layer can induce uniform Li^+ flow and promote Li^+ transmission, ensuring uniform Li nucleation/dissolution; (3) the PVA–PAA coating layer possesses high binding ability to closely combine with Li and alleviate the dimensional variation over multiple cycles. Consequently, a dense Li anode with dendrite-free morphology can be achieved even after long-term cycling. In short, using such a multifunctional artificial protective layer can be a promising strategy to address the non-uniform deposition and dendrite growth in the anode of practical LMBs.

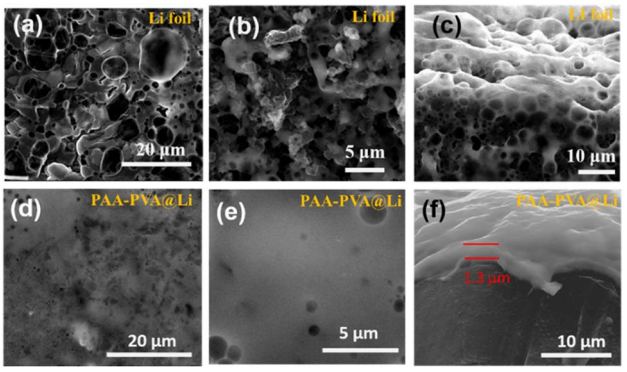

Fig. 6 SEM images of (a–c) bare Li anodes and (d–f) PVA–PAA coated Li after 50 cycles at 1 mA cm^{-2} with a fixed capacity of 1 mA h cm^{-2}.

Author contributions

Chaohui Wei: conceptualization, investigation, and writing – original draft. Jinxiang Deng: data curation and methodology. Jianxiong Xing: data curation. Zihang Wang: data curation. Zhicui Song: data curation. Donghuang Wang: methodology and validation. Jicheng Jiang: supervision and formal analysis. Xin Wang: visualization. Aijun Zhou: conceptualization, supervision, and funding acquisition. Wei Zou: supervision and funding acquisition. Jingze Li: supervision, funding acquisition, and writing – review & editing.

Conflicts of interest

The authors declare that they have no known competing financial interests or personal relationships that could have appeared to influence the work reported in this paper.

Acknowledgements

This work is partly supported by the National Natural Science Foundation of China (No. 21673033 and 52172184).

Notes and references

1 J. B. Goodenough and Y. Kim, *Chem. Mater.*, 2010, **22**, 587–603.
2 X. Wu, J. Wang, D. Fei, X. Chen, E. Nasybulin, Y. Zhang and J. Zhang, *Energy Environ. Sci.*, 2014, **7**, 513–537.
3 D. Lin, Y. Liu and Y. Cui, *Nat. Nanotechnol.*, 2017, **12**, 194–206.
4 P. Shi, X. Zhang, X. Shen, R. Zhang, H. Liu and Q. Zhang, *Adv. Mater. Technol.*, 2019, 1900806.
5 J. Li, Z. Kong, X. Liu, B. Zheng, Q. H. Fan, E. Garratt, T. Schuelke, K. Wang, H. Xu and H. Jin, *InfoMat*, 2021, **3**, 1333–1363.
6 D. Kang, S. Sardar, R. Zhang, H. Noam, J. Chen, L. Ma, W. Liang, C. Shi and J. P. Lemmon, *Energy Storage Mater.*, 2020, **27**, 69–77.
7 Y. Yang, J. Xiong, S. Lai, R. Zhou, M. Zhao, H. Geng, Y. Zhang, Y. Fang, C. Li and J. Zhao, *ACS Appl. Mater. Interfaces*, 2019, **11**, 6118–6125.
8 F. Jiang, X. Cheng, S. Yang, J. Xie, H. Yuan, L. Liu, J. Huang and Q. Zhang, *Adv. Mater.*, 2023, **35**, 2209114.
9 Y. Zhang, L. Yu, X. D. Zhang, Y. H. Wang, C. P. Yang, X. L. Liu, W. P. Wang, Y. Zhang, X. T. Li, G. Li, S. Xin, Y. G. Guo and C. L. Bai, *Sci. Adv.*, 2023, **9**, ade5802.
10 A. Yang, C. Yang, K. Xie, S. Xin, Z. Xiong, K. Li, Y.-G. Guo and Y. You, *ACS Energy Lett.*, 2023, **8**, 836–843.
11 C. Lu, M. Tian, X. Zheng, C. Wei, M. H. Rummeli, P. Strasser and R. Yang, *Chem. Eng. J.*, 2022, **430**, 132722.
12 Y. Liao, L. Yuan, J. Xiang, W. Zhang, Z. Cheng, B. He, Z. Li and Y. Huang, *Nano Energy*, 2020, **69**, 104471.
13 J. Gao, C. Chen, Q. Dong, J. Dai, Y. Yao, T. Li, A. Rundlett, R. Wang, C. Wang and L. Hu, *Adv. Mater.*, 2021, **33**, 2005305.
14 X. Gu, J. Dong and C. Lai, *Eng. Rep.*, 2021, **3**, e12339.
15 R. Zhang, X. Chen, X. Shen, X. Zhang, X. Chen, X. Cheng, C. Yan, C. Zhao and Q. Zhang, *Joule*, 2018, **2**, 764–777.
16 Y. Liang, Y. Xiao, C. Yan, R. Xu, J. Ding, J. Liang, H.-J. Peng, H. Yuan and J. Huang, *J. Energy Chem.*, 2020, **48**, 203–207.
17 Y. Yang, J. Xiong, S. Lai, R. Zhou, M. Zhao, H. Geng, Y. Zhang, Y. Fang, C. Li and J. Zhao, *ACS Appl. Mater. Interfaces*, 2019, **11**, 6118–6125.
18 Y. Shuai, Z. Zhang, K. Chen, J. Lou and Y. Wang, *Chem. Commun.*, 2019, **55**, 2376–2379.
19 L. Fan, Z. Guo, Y. Zhang, X. Wu, C. Zhao, X. Sun, G. Yang, Y. Feng and N. Zhang, *J. Mater. Chem. A*, 2020, **8**, 251–258.
20 K. Li, Y. Wang, W. Jia, S. Qu, Z. Yao, R. Cui, W. Zou, F. Zhou and J. Li, *ACS Appl. Mater. Interfaces*, 2020, **12**, 2285–2292.
21 L. Wang, L. Zhang, Q. Wang, W. Li, B. Wu, W. Jia, Y. Wang, J. Li and H. Li, *Energy Storage Mater.*, 2018, **10**, 16–23.
22 W. Liu, W. Li, D. Zhuo, G. Zheng, Z. Lu, K. Liu and Y. Cui, *ACS Cent. Sci.*, 2017, **3**, 135–140.
23 N. W. Li, Y. X. Yin, C. P. Yang and Y. G. Guo, *Adv. Mater.*, 2016, **28**, 1853–1858.
24 L. Wang, Q. Wang, W. Jia, S. Chen, P. Gao and J. Li, *J. Power Sources*, 2017, **342**, 175–182.
25 Y. Yuan, F. Wu, Y. Bai, Y. Li, G. Chen, Z. Wang and C. Wu, *Energy Storage Mater.*, 2019, **16**, 411–418.
26 K. Chen, R. Pathak, A. Gurung, E. A. Adhamash, B. Bahrami, Q. He, H. Qiao, A. L. Smirnova, J. J. Wu, Q. Qiao and Y. Zhou, *Energy Storage Mater.*, 2019, **18**, 389–396.
27 J. Deng, Y. Wang, S. Qu, Y. Liu, W. Zou, F. Zhou, A. Zhou and J. Li, *Batteries Supercaps*, 2021, **4**, 140.
28 Y. Lin, Z. Wen, C. Yang, P. Zhang and J. Zhao, *Electrochem. Commun.*, 2019, **108**, 106565.
29 S. Qu, W. Jia, Y. Wang, C. Li, Z. Yao, K. Li, Y. Liu, W. Zou, F. Zhou, Z. Wang and J. Li, *Electrochim. Acta*, 2019, **317**, 120–127.
30 W. Tang, X. Yin, S. Kang, Z. Chen, B. Tian, S. L. Teo, X. Wang, X. Chi, K. P. Loh, H. W. Lee and G. W. Zheng, *Adv. Mater.*, 2018, **30**, 1801745.
31 A. A. Assegie, J. H. Cheng, L. M. Kuo, W. N. Su and B. Hwang, *Nanoscale*, 2018, **10**, 6125–6138.
32 H. Wu, Z. Yao, Q. Wu, S. Fan, C. Yin and C. Li, *J. Mater. Chem. A*, 2019, **7**, 22257–22264.
33 S. Yang, N. Yao, F. Jiang, J. Xie, S. Sun, X. Chen, H. Yuan, X. Cheng, J. Huang and Q. Zhang, *Angew. Chem., Int. Ed.*, 2022, **61**, e202214545.
34 S. Li, Y. Huang, C. Luo, W. Ren, J. Yang, X. Li, M. Wang and H. Cao, *Chem. Eng. J.*, 2020, **399**, 125687.
35 J. Luo, C. Fang and N. Wu, *Adv. Energy Mater.*, 2018, **8**, 1701482.
36 J. Lopez, A. Pei, J. Y. Oh, G. N. Wang, Y. Cui and Z. Bao, *J. Am. Chem. Soc.*, 2018, **140**, 11735.
37 X. Ma, H. Chen, X. Liu, Y. Li, C. Li, S. Zhang, H. Lin and H. Wang, *Macromol. Mater. Eng.*, 2022, **307**, 2100923.
38 C. Fu and C. Battaglia, *ACS Appl. Mater. Interfaces*, 2020, **12**, 41620–41626.
39 Y. Liu, D. Lin, P. Y. Yuen, K. Liu, J. Xie, R. H. Dauskardt and Y. Cui, *Adv. Mater.*, 2017, **29**, 1605531.
40 Y. Zhao, D. Wang, Y. Gao, T. Chen, Q. Huang and D. Wang, *Nano Energy*, 2019, **64**, 103893.

41 G. Wang, C. Chen, Y. Chen, X. Kang, C. Yang, F. Wang, Y. Liu and X. Xiong, *Angew. Chem., Int. Ed.*, 2020, **59**, 2055–2060.
42 G. Liu, Y. Li, L. Zhang, H. Tao and X. Yang, *Appl. Surf. Sci.*, 2023, **620**, 156809.
43 N. Li, Y. Shi, Y. X. Yin, X. X. Zeng, J. Y. Li, C. J. Li, L. J. Wan, R. Wen and Y. Guo, *Angew. Chem., Int. Ed.*, 2018, **57**, 1505–1509.
44 Y. Wang, L. Ren, J. Liu, X. Lu, Q. Wang, M. Zhou, W. Liu and X. Sun, *ACS Appl. Mater. Interfaces*, 2022, **14**, 50982–50991.
45 Y. Feng, C. Zhang, X. Jiao, Z. Zhou and J. Song, *Energy Storage Mater.*, 2020, **25**, 172–179.
46 L. Wang, L. Zhang, Q. Wang, W. Li, B. Wu, W. Jia, Y. Wang, J. Li and H. Li, *Energy Storage Mater.*, 2018, **10**, 16–23.
47 Z. Wang, Z. Song, Y. Liu, J. Xing, C. Wei, W. Zou and J. Li, *Phys. Chem. Chem. Phys.*, 2023, **25**, 124.